Comparative diffusion coefficients of major and trace elements in olivine at ~950 °C from a xenocryst included in dioritic magma

Qing Qian[1,2], Hugh St.C. O'Neill[2], and Jörg Hermann[2]
[1]Key Laboratory of Mineral Resources, Institute of Geology and Geophysics, Chinese Academy of Sciences, Beijing 100029, China
[2]Research School of Earth Sciences, The Australian National University, Canberra, ACT 0200, Australia

ABSTRACT

The concentration profiles of 13 trace elements (Li, Na, Al, P, Ca, Sc, Ti, V, Cr, Mn, Co, Ni, and Y) were determined in a natural mantle olivine xenocryst included in a hybridized hydrous dioritic magma during cooling from ~1000 °C, which allow trace-element chemical diffusion coefficients to be evaluated relative to Mg-Fe interdiffusion under conditions that are difficult to access in the laboratory. The effective diffusion coefficients of many elements (Li, Ca, Sc, Mn, Co, Ni, and Y) fell within a factor of three of the corresponding Mg-Fe interdiffusion coefficient, in agreement with results from laboratory experiments at higher temperatures. By contrast, the concentration profiles for Na, Ti, and V implied much faster diffusion rates, while P showed no discernible diffusion. The Al and Cr profiles, which were well correlated with each other, were complex and variable on a small length scale due to local precipitation of spinel. These data show that the diffusion coefficients of cations in olivine are not simple functions of ionic charge or ionic radius, but they are likely controlled by the availability of suitable diffusion pathways.

INTRODUCTION

Despite the fact that solid-state diffusion is central to many geological processes, little is known about the factors controlling the rates of diffusion of trace elements in silicate minerals. In particular, there is a general paucity of empirical data against which theoretical models might be tested. Much of what is known about diffusion in silicates concerns the mineral olivine, as Chakraborty (2008) pointed out in a recent review. The diffusivities of major elements and several compatible trace elements in ferromagnesian olivine have been determined experimentally by a variety of techniques (Petry et al., 2004; Coogan et al., 2005; Dohmen and Chakraborty, 2007), and those of some incompatible trace elements, including rare earth elements (REEs), were recently reported from experiments at 1300 °C in which natural olivine phenocrysts were immersed in a synthetic basaltic melt (Spandler et al., 2007). In the latter study, the high temperature (1300 °C) enabled long diffusion profiles (~200 μm) to be generated in experimentally reasonable times (~25 d), allowing the diffusion profiles to be measured along transverse sections using the well-established geochemical microanalytical methods of the electron microprobe (EMP) and laser-ablation–inductively coupled plasma–mass spectroscopy (LA-ICP-MS). Despite differences in ionic size and charge, it was found that the REEs, Sc, and Ti all diffuse at approximately similar rates to Mg and Fe and other divalent cations (Ni and Mn), and the same result has recently been supported by similar experiments using San Carlos olivine (Spandler and O'Neill, 2010). The method has the great advantage that the chemical potentials of all components can be fixed, which is a prerequisite for studying those trace elements for which substitution into a crystal requires some means of charge balance. In addition, the concentrations of the trace elements at the crystal-melt interface yield partition coefficients that may be checked against those obtained from equilibrium partitioning experiments, to test whether the concentrations of the diffusing elements are compatible with equilibrium substitution mechanisms. The method's disadvantage is that relatively long diffusion profiles (>100 μm) are needed, which has prevented it being used in laboratory experiments at low temperatures where only short profiles could be generated in reasonable times. However, xenocrysts included in an exotic magma constitute a natural diffusion experiment of this type, in which concentration profiles of a suitable length can develop on geological as opposed to laboratory time scales (Costa and Chakraborty, 2004; Costa and Dungan, 2005). Here, we use a particularly propitious occurrence of diffusion profiles generated in olivine xenocrysts of upper-mantle composition immersed in a dioritic magma to constrain the rates of diffusion relative to Mg-Fe interdiffusion of several key trace elements (Li, Na, P, Ca, Sc, Ti, V, Mn, Co, Ni, and Y) at natural concentrations and at a temperature well below that practicable in the laboratory.

GEOLOGICAL CONTEXT

The olivine xenocrysts (0.5–3 mm in diameter, up to 6% by volume) were found in the chilled margin of one of the plutons of high-Mg diorite from Handan-Xingtai, central North China block, which was formed at an intracontinental setting at 134.2 ± 1.3 Ma (our unpublished sensitive high-resolution ion microprobe [SHRIMP] zircon U-Pb data). The suite of diorites shows in their chemistry the effects of variable assimilation of upper-mantle peridotite (relict harzburgite xenoliths were described elsewhere in these plutons by Huang and Xue [1990]), starting from an initial magma with ~2 wt% MgO (see Appendix DR1 and Table DR1 in the GSA Data Repository[1] for further details). Some olivine crystals display kink bands or undulatory extinction from deformation that predates the zoning; rare olivine aggregates are also found (Appendix DR3).

The olivine xenocrysts are surrounded by a corona (40–60 μm wide) of interweaved microcrystalline orthopyroxene and spinel (Fig. 1). Euhedral chromite occurs next to the margin of olivine, and quartz exists in the groundmass even within 100 μm of the olivine. All these textural observations provide evidence that the olivines are xenocrysts in disequilibrium with the groundmass diorite. Assuming a pressure of ~0.4 GPa from Al-in-amphibole geobarometry (Schmidt, 1992), the two-pyroxene geothermometer of Brey and Köhler (1990) gives 1000 °C for neoblastic pyroxenes at the olivine rim and 850 °C for the groundmass, approximating liquidus and near-solidus temperatures, respectively (Murphy et al., 2000). The redox state is $\log fO_2 = QFM + 0.5$ to $+ 1.0$, where QFM is the quartz-fayalite-magnetite oxygen buffer (O'Neill and Wall, 1987). A relatively high H_2O content of the magma is inferred from the occurrence of amphibole and biotite.

CONCENTRATION PROFILES AND RELATIVE DIFFUSION COEFFICIENTS

Olivine xenocrysts were normally zoned in Mg/Fe, with forsterite content (Fo, molar 100 × Mg/[Mg + Fe^T]) decreasing from core (89.1–93.2) to rim (73.2–81.4). The xenocrysts cover a range of sizes and show textures evident of various degrees of reaction with the magma. One exceptional crystal with favorable dimension and orientation, and still retaining a crystal face, indicating minimal dissolution, was selected for detailed study (Fig. 1). Concentration profiles of

---

[1]GSA Data Repository item 2010088, Appendices DR1–DR3 and Tables DR1–DR4, is available online at www.geosociety.org/pubs/ft2010.htm, or on request from editing@geosociety.org or Documents Secretary, GSA, P.O. Box 9140, Boulder, CO 80301, USA.
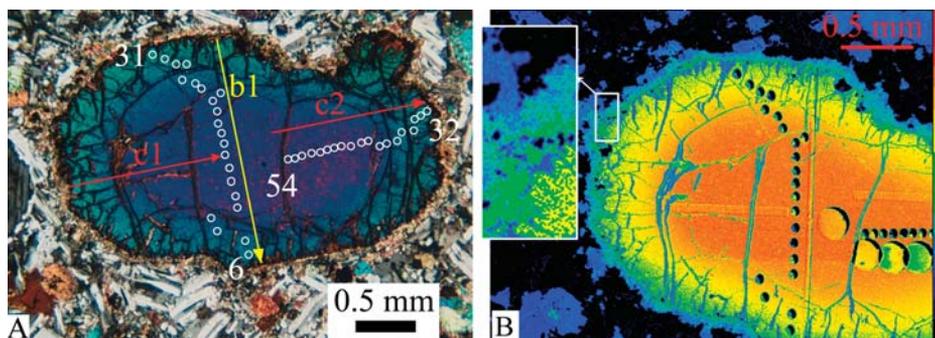
Figure 1. A: Olivine xenocryst CS32-ol under polarized light. B: X-ray map of Mg for part of CS32-ol. In A, arrows mark analytical traverses by laser-ablation–inductively coupled plasma–mass spectroscopy (LA-ICP-MS) with a rectangular beam. Traverse b1 is along [010] (data shown in Figs. 2A–2E), and c1 and c2 are along [001]. White circles mark positions of LA-ICP-MS spot analyses (Table DR4 [see footnote 1]). The insert in B is an enlargement of an olivine rim, showing the thin corona of orthopyroxene (green in color) and clinopyroxene (blue). Late serpentine veins appear in blue color and did not affect diffusion zoning.

Mg, Fe, Mn and Ni were determined by electron microprobe (Table DR2), and concentration profiles of trace elements (Li, Na, Al, P, Ca, Sc, Ti, V, Cr, Mn, Co, Ni, and Y; Tables DR3 and DR4) were determined along the same or similar paths by LA-ICP-MS. Analytical methods are given in Appendix DR2.

The core of our selected olivine xenocryst has typical Ni (~3500 ppm) and Mn (~630 ppm) values for mantle olivine, with low Ca (<400 ppm), low Al (<200 ppm), but moderate Cr (300–350 ppm), indicating, together with the relatively high Fo (93), a provenance from highly depleted peridotite (harzburgite or dunite). The concentrations of the incompatible elements P (~16 ppm), Sc (~2.3 ppm), and Y (6 ppb) in the core are below those of the mantle olivines analyzed by Witt-Eickschen and O'Neill (2005) (P: 20–160 ppm; Sc: 2.3–4.8 ppm; Y: 12–76 ppb), which agrees with the depleted diagnosis. We thus have an olivine from a source strongly depleted in incompatible elements immersed in a reservoir, the dioritic magma, that is enriched in these elements (Table DR1).

Mapping of major elements reveals gradual changes in olivine composition (Fig. 1B) similar to previous reports of diffusion in natural olivines (Costa and Dungan, 2005) and quite unlike the zonation found in overgrowths on olivine phenocrysts (see Kamenetsky et al., 2008, and references therein). The rim-to-core concentrations of major, minor, and trace elements decrease smoothly from values appropriate for crystal-liquid partitioning to core concentrations typical of mantle olivine, providing further evidence that the investigated grain represents a mantle xenocryst modified by diffusion. Representative concentration profiles (plotted as Fo) along [010] and [001] are given in Figure 2A. The Mg-Fe zoning in a rare polycrystalline aggregate of olivines, in which each olivine has

slightly different initial Mg#, shows the same steep gradients in Mg# toward those boundaries that are in contact with the diorite, but subtle gradients along similar length scales either side of the olivine-olivine contacts, demonstrating olivine-to-olivine diffusion (Appendix DR3).

The solution to Fick's Laws for one-dimensional diffusion into a semi-infinite medium with constant concentration at a fixed crystal-melt boundary and a constant diffusion coefficient, D, is:

$$erfc^{-1}\left(\frac{c(x)-c_o}{c_i-c_o}\right) = \frac{x}{2(Dt)^{1/2}}, \quad (1)$$

where $c(x)$ is the concentration at distance x, c_i is the concentration at the interface ($x = 0$), which is taken to be the boundary of the crystal as presently observed, c_o is the initial concentration, and t is the residence time. Diffusion would have occurred over a range of temperatures, which can be modeled by invoking a characteristic temperature that is equivalent to ~95% of the maximum temperature in Kelvins (Chakraborty and Ganguly, 1991).

Potential complications in the interpretation of the measured concentration profiles include the movement of the boundary of the olivine-melt interface as the olivine dissolves, although the amount of olivine lost from our selected crystal, judging from its shape, is small compared to both its original dimensions and to the concentration profiles of interest. Dissolution of the olivine may change the composition of the melt, although this effect is minor for trace elements that are incompatible in olivine. For these reasons, plots of the left-hand side of Equation 1 versus x may deviate from the straight line expected from the simple model of Equation 1. However, even for Mg-Fe interdiffusion, the deviations are not large (Fig. 3A).
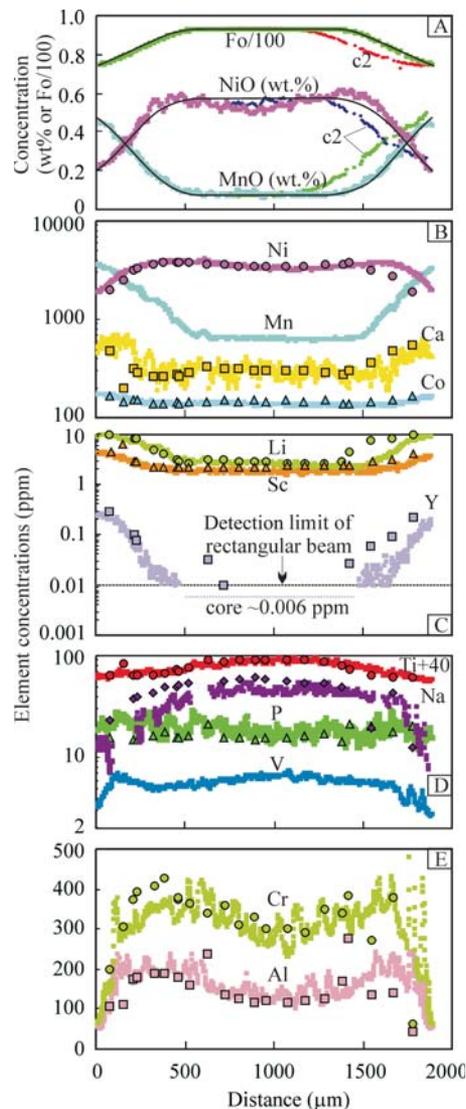
Figure 2. Diffusion profiles along [010] (traverse b1 in Fig. 1A). A: Electron microprobe (EMP) analyses of Mg-Fe (as Fo/100), NiO, and MnO. Profiles of Fo, NiO, and MnO along [001] from traverse c2 are also shown. Black curves are model fits to these data at 1210 K (i.e., ~95% of 1273 K) and log fO$_2$ = QFM + 0.5, using diffusion coefficients as summarized by Costa and Dungan (2005). In B to E, circles, squares, triangles, and diamonds with black rims are spots by laser-ablation–inductively coupled plasma–mass spectroscopy (LA-ICP-MS) analyses, and colored symbols plot LA-ICP-MS traverses with rectangular beam. Profiles for Ti are shown as Ti plus 40 ppm to separate data from Na.

Mn (Fig. 3B), the most precisely determined trace element, shows a good linear trend.

The concentration profiles for Li, Ca, Sc, Co, and Y are similar in shape to those of Mn (Figs. 2B and 2C), and also give reasonably straight lines when fitted to Equation 1 (Fig. 3). For these elements, the ratio of the slopes from these fits to the slope for Mn (here chosen as the
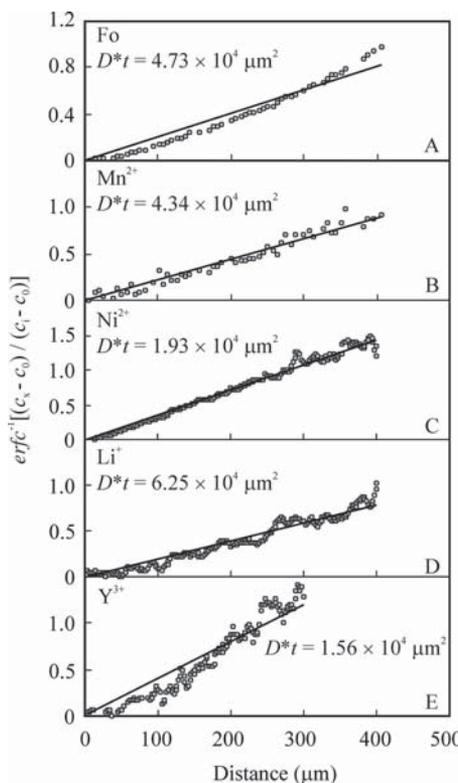
Figure 3. Plots of $erfc^{-1}\left(\dfrac{c(x)-c_o}{c_i-c_o}\right)$ versus distance (*x*) from olivine-melt interface for Fo (i.e., Mg-Fe interdiffusion), Mn, Ni, Li, and Y (see Eq. 1), from top half of traverse b1 shown in Figure 1A. Deviation from a straight line for Fo data is expected from dependence of interdiffusion coefficient $D_{Mg\text{-}Fe}$ on Fo (Dohmen and Chakraborty, 2007). Mg, Fe, and Mn were analyzed by electron microprobe (EMP); other elements were analyzed by laser-ablation–inductively coupled plasma–mass spectroscopy (LA-ICP-MS) by scanning with rectangular beam.

TABLE 1. COMPARATIVE DIFFUSION COEFFICIENTS RELATIVE TO Mn (i.e., D_M/D_{Mn})

Profile	Description	Li	Ca	Sc	Co	Ni	Y	Mg-Fe*	Ni*
c1	//*c* axis	2.0	–	1.1	1.1	1.2	0.4	1.2	1.0
c2	//*c* axis	4.0	0.5	1.0	1.0	1.1	0.8	1.5	0.6
b1–1	//*b* axis	1.4	0.6	0.5	0.7	0.4	0.4	1.1	0.6
b1–2	//*b* axis	1.1	0.6	0.8	0.4	0.6	0.3	1.1	0.5

*Electron microprobe; – —not calculated.

the olivine. In detail, the concentration profile is saddle-shaped, possibly caused by a dependence of D_{Ni} on Fo, or by the buildup of Ni in the melt from dissolution of other olivines. The ratio D_{Ni}/D_{Mn} obtained from a fit of the data to Equation 1 (see Fig. 3C) is 0.8, which agrees with the slower diffusion of Ni compared to Mn in the higher-temperature laboratory experiments (e.g., Petry et al., 2004; Spandler and O'Neill, 2010). Diffusion for all these elements is faster along the *c* axis compared to the *b* axis (Figs. 1A and 2B; Tables DR2, DR3, and DR4). For example, the profiles for Fo, Ni, and Mn extend further into the olivine along [001] than along [010] (Fig. 2A), consistent with the diffusion anisotropy observed in laboratory experiments (Petry et al., 2004; Dohmen and Chakraborty, 2007; Spandler and O'Neill, 2010) and other natural examples (Costa and Chakraborty, 2004).

The concentration profiles of Na, Ti, and V are quite different (Fig. 2D), decreasing toward the rim despite the incompatible nature of these elements in olivine and their high concentration in the dioritic magma. The core concentrations of both Ti (50 ppm) and V (6.8 ppm) are higher than in all but one of the olivines analyzed by Witt-Eickschen and O'Neill (2005; Ti, 13–80 ppm; V, 5.7–7.5 ppm). The core Ti/Y ratio of 10^4 is one to two orders of magnitude higher than that found in mantle olivines (Witt-Eickschen and O'Neill, 2005). Moreover, concentrations of these three elements decrease on approach to the rim, which is opposite to the other incompatible elements discussed previously herein. Taken together, these observations imply that diffusion of Na, Ti, and V in the olivine was so fast as to allow initially for these elements to achieve full metastable equilibrium between the olivine and the dioritic melt; further cooling then results in back diffusion of Na, Ti, and V out of the rim of the olivine. The inference is that D_{Na}, D_{Ti}, and D_V are orders of magnitude faster than $D_{Mg\text{-}Fe}$.

Phosphorus does not show core-to-rim zoning despite the high P content of the dioritic melt, confirming that the diffusion of this element in olivine is particularly sluggish (Spandler et al., 2007). The concentrations of Al and Cr are variable but correlated with each other (Fig. 2E). Notably, the concentrations of both elements decrease sharply near the rim of the crystal, e.g., Al dwindles to a very low level (~50 ppm). The decrease of Al is not expected for local diffusive equilibration with a dioritic melt, for which relatively high alumina activity ought to promote diffusion of Al into the olivine. The profiles obtained by LA-ICP-MS in the scanning mode reveal short-scale fluctuations in Al and Cr abundances in all parts of the profile. We interpret the correlated Al-Cr profiles as due to a combination of three factors: (1) the substitution of Cr and Al is coupled as an $MCrAlO_4$ (M = Mg or Fe^{2+}) component (Witt-Eickschen and O'Neill, 2005); (2) the concentrations of both elements are then controlled by very slow diffusion of Al (Spandler et al., 2007); and (3) the decrease of both elements at the rim of the crystal is a result of precipitation of spinel on a local scale, caused by the flux of Fe into the olivine.

DISCUSSION

With the assumption of the physical conditions discussed already, the anhydrous diffusion coefficients $D_{Mg\text{-}Fe}$, D_{Ni}, and D_{Mn} summarized in Petry et al. (2004), Coogan et al. (2005), and Dohmen and Chakraborty (2007) were used to model the time needed to produce the diffusion profile measured along [010] as ~10^3 yr. Allowing for an increase in diffusion coefficients of about one order of magnitude for the high fH_2O of the system (Wang et al., 2004) would reduce this time to ~10^2 yr. Dissolution experiments at high temperatures (>1200 °C) show that mantle xenolith and forsterite are preserved in basaltic and andesitic melts only for several days (Donaldson, 1990); the present observation implies that olivine xenocrysts can survive for substantially longer times in cooler dioritic magma.

That olivine dissolution was slow compared to diffusion is the key factor in permitting the long concentration profiles to develop, which we have exploited to constrain relative diffusion rates under the physical conditions discussed here. For the divalent elements Ca, Co, and Ni, and for Mg-Fe interdiffusion, the rates relative to Mn diffusion closely resemble those obtained from laboratory experiments at higher temperatures and low fH_2O, arguing that both the activation energies and the dependence of diffusion on H_2O-associated defects are similar for all these divalent elements. This natural experiment also confirms that the diffusion rates of Y (a good proxy for REE) and Sc are similar to those of the divalent cations,

reference) should be approximately $(D_M/D_{Mn})^{-1/2}$, as the time is the same, and the effect of the moving interface caused by dissolution should affect M and Mn more-or-less equally. Hence, diffusion rates for these elements may be quantified relative to Mn (Table 1). Diffusion rates for the divalent cations Ca and Co relative to Mn are similar to those observed in laboratory experiments at higher temperature (Morioka, 1981; Petry et al., 2004; Coogan et al., 2005). It is noteworthy that D_{Li}, D_{Sc}, and D_Y are similar in magnitude to D_{Mn}, in agreement with laboratory experiments at 1300 °C, 1 bar, and very low fH_2O (Spandler et al., 2007; Spandler and O'Neill, 2010).

Nickel, with initial concentrations of ~3500 ppm in the olivine (typical for mantle olivine) but a low concentration in the parent dioritic magma (Table DR1), diffuses out of

in agreement with Spandler et al. (2007) and Spandler and O'Neill (2009) at 1300 °C.

Diffusion of Li through the silicate minerals of the upper mantle may cause fractionation of Li isotopes at high temperatures (e.g., Parkinson et al., 2007). Therefore, an important result is that the diffusion rate of Li into olivine is similar to that of the divalent cations, as found by Spandler and O'Neill (2009), who studied the diffusion of Li out of dry olivine at 1300 °C, and of Parkinson et al. (2007) on olivine phenocrysts in primitive arc lavas. The diffusion coefficient of Li in olivine depends strongly on Li concentration (Dohmen et al., 2010), providing an excellent example of the need of minerals in trace-element diffusion studies to ensure that the concentration ranges studied are relevant to the substitution mechanisms occurring in nature.

Rather unexpectedly, given its comparatively slow diffusion in the anhydrous, high-temperature experiments (Spandler and O'Neill, 2009), the concentration profiles for Na imply much faster diffusion than for Li. Fast diffusion is also observed for Ti and V, as at high temperature (Spandler and O'Neill, 2009). For Ti, the fast rate may reflect its occupation in both tetrahedral and octahedral sites (Hermann et al., 2005, 2007). The presence of two such different substitution mechanisms gives a much greater density of diffusion pathways than would be available for an element confined to a single site. Analogous considerations may apply to V on account of the variable oxidation state of this element; presumably V^{5+} with its high charge but small ionic radius would substitute for Si^{4+} on the tetrahedral sites, with V^{3+} and V^{4+} on octahedral sites.

Our results show that expectations based on simple considerations of ionic radius and ionic charge may be misleading in predicting relative diffusion rates in silicate minerals. Rather, diffusion of incompatible trace elements in silicates is likely controlled by the requirements of stoichiometry and charge balance, and, as Chakraborty (2008) pointed out in his recent review, the availability of vacancies. Hence, different cations making use of the same vacancies would be expected to diffuse at approximately similar rates regardless of ionic charge or radius, as observed previously in higher-temperature, dry experiments by Spandler et al. (2007) and Spandler and O'Neill (2009).

REFERENCES CITED
Brey, G.P., and Köhler, T., 1990, Geothermobarometry in four-phase lherzolites: II. New thermobarometers, and practical assessment of existing thermobarometers: Journal of Petrology, v. 31, p. 1353–1378.
Chakraborty, S., 2008, Diffusion in solid silicates: A tool to track timescales of processes comes of age: Annual Review of Earth and Planetary Sciences, v. 36, p. 153–190, doi: 10.1146/annurev.earth.36.031207.124125.
Chakraborty, S., and Ganguly, J., 1991, Compositional zoning and cation diffusion in aluminosilicate garnets, in Ganguly, J., ed., Diffusion, Atomic Ordering and Mass Transport—Selected Topics in Geochemistry (Advances in Physical Geochemistry, 8): Berlin, Springer-Verlag, p. 120–175.
Coogan, L.A., Hain, A., Stahl, S., and Chakraborty, S., 2005, Experimental determination of the diffusion coefficient for calcium in olivine between 900 °C and 1500 °C: Geochimica et Cosmochimica Acta, v. 69, p. 3683–3694, doi: 10.1016/j.gca.2005.03.002.
Costa, F., and Chakraborty, S., 2004, Decadal time gaps between mafic intrusion and silicic eruption obtained from chemical zoning patterns in olivine: Earth and Planetary Science Letters, v. 227, p. 517–530, doi: 10.1016/j.epsl.2004.08.011.
Costa, F., and Dungan, M., 2005, Short time scales of magmatic assimilation from diffusion modeling of multiple elements in olivine: Geology, v. 33, p. 837–840, doi: 10.1130/G21675.1.
Dohmen, R. and Chakraborty, S., 2007, Fe-Mg diffusion in olivine: II. Point defect chemistry, change of diffusion mechanisms and a model for calculation of diffusion coefficients in natural olivine: Physics and Chemistry of Minerals, v. 34, p. 409–430, doi: 10.1007/s00269-007-0158-6.
Dohmen, R., Kasemann, S.A., Coogan, L., and Chakraborty, S., 2010, Diffusion of Li in olivine, Part I: Experimental observations and a multi-species diffusion model: Geochimica et Cosmochimica Acta, v. 74, p. 274–292, doi: 10.1016/j.gca.2009.10.016.
Donaldson, C.H., 1990, Forsterite dissolution in superheated basaltic andesitic and rhyolitic melts: Mineralogical Magazine, v. 54, p. 67–74, doi: 10.1180/minmag.1990.054.374.06.
Hermann, J., O'Neill, H.St.C., and Berry, A.J., 2005, Titanium solubility in olivine in the system TiO$_2$-MgO-SiO$_2$: No evidence for an ultra-deep origin of Ti-bearing olivine: Contributions to Mineralogy and Petrology, v. 148, p. 746–760, doi: 10.1007/s00410-004-0637-4.
Hermann, J., Fitz Gerald, J., Malaspina, N., Berry, A.J., and Scambelluri, M., 2007, OH-bearing planar defects in olivine produced by the breakdown of Ti-rich humite minerals from Dabie Shan (China): Contributions to Mineralogy and Petrology, v. 153, p. 417–428, doi: 10.1007/s00410-006-0155-7.
Huang, F.S., and Xue, S.Z., 1990, The discovery of the mantle-derived ultramafic xenoliths in Handan Xingtai intrusive complex and their mineralogical-geochemical characteristics: Acta Petrologica Sinica, v. 4, p. 40–45 (in Chinese with English abstracts).
Kamenetsky, V.S., Kamenetsky, M.B., Sobolev, A.V., Golovin, A.V., Demouchy, S., Faure, K., Sharygin, V.V., and Kuzmin, D.V., 2008, Olivine in the Udachnaya-east kimberlite (Yakutia, Russia): Types, compositions and origins: Journal of Petrology, v. 49, p. 823–839, doi: 10.1093/petrology/egm033.
Morioka, M., 1981, Cation diffusion in olivine. 2. Ni-Mg, Mn-Mg, Mg and Ca: Geochimica et Cosmochimica Acta, v. 45, p. 1573–1580, doi: 10.1016/0016-7037(81)90286-6.
Murphy, M.D., Sparks, R.S.J., Barclay, J., Carroll, M.R., and Brewer, T.S., 2000, Remobilization of andesite magma by intrusion of mafic magma at the Soufriere Hills Volcano, Montserrat, West Indies: Journal of Petrology, v. 41, p. 21–42, doi: 10.1093/petrology/41.1.21.
O'Neill, H.St.C., and Wall, V.J., 1987, The olivine-orthopyroxene-spinel oxygen geobarometer, the nickel precipitation curve, and the oxygen fugacity of the Earth's upper mantle: Journal of Petrology, v. 28, p. 1169–1191.
Parkinson, I.J., Hammond, S.J., James, R.H., and Rogers, N.W., 2007, High-temperature lithium isotope fractionation: Insights from lithium isotope diffusion in magmatic systems: Earth and Planetary Science Letters, v. 257, p. 609–621, doi: 10.1016/j.epsl.2007.03.023.
Petry, C., Chakraborty, S., and Palme, H., 2004, Experimental determination of Ni diffusion coefficients in olivine and their dependence on temperature, composition, oxygen fugacity, and crystallographic orientation: Geochimica et Cosmochimica Acta, v. 68, p. 4179–4188, doi: 10.1016/j.gca.2004.02.024.
Schmidt, M.W., 1992, Amphibole composition in tonalite as a function of pressure: An experimental calibration of the Al-in-hornblende barometer: Contributions to Mineralogy and Petrology, v. 110, p. 304–310, doi: 10.1007/BF00310745.
Spandler, C., and O'Neill, H.St.C., 2010, Diffusion and partition coefficients of minor and trace elements in San Carlos olivine at 1300 °C with some geochemical implications: Contributions to Mineralogy and Petrology (in press), doi: 10.1007/s00410-009-0456-8.
Spandler, C., O'Neill, H.St.C., and Kamenetsky, V.S., 2007, Survival times of anomalous melt inclusions from element diffusion in olivine and chromite: Nature, v. 447, p. 303–306, doi: 10.1038/nature05759.
Wang, Z.Y., Hiraga, T., and Kohlstedt, D.L., 2004, Effect of H^+ on Fe-Mg interdiffusion in olivine, (Fe, Mg)$_2$SiO$_4$: Applied Physics Letters, v. 85, p. 209–211, doi: 10.1063/1.1769593.
Witt-Eickschen, G., and O'Neill, H.St.C., 2005, The effect of temperature on the equilibrium distribution of trace elements between clinopyroxene, orthopyroxene, olivine and spinel in upper mantle peridotite: Chemical Geology, v. 221, p. 65–101, doi: 10.1016/j.chemgeo.2005.04.005.